Fundamental study of mechanical energy harvesting using piezoelectric nanostructures

Chengliang Sun, Jian Shi, and Xudong Wang[a)]
Department of Materials Science and Engineering, University of Wisconsin at Madison, Madison, Wisconsin 53706, USA

(Received 30 April 2010; accepted 12 June 2010; published online 5 August 2010)

This paper numerically estimates the potential, the output power and the energy conversion efficiency of piezoelectric nanostructures, including rectangular nanowires (NWs), hexagonal NWs, and two-dimensional vertical thin films (the nanofins). Static analysis studies the maximum piezoelectric potential that can be produced by a $BaTiO_3$ NW, a ZnO NW, and a ZnO nanofin when they are subjected to a constant external force. Dynamic analysis is performed to study the power generation ability via the vibration of these nanostructures agitated by ambient vibration energy. ZnO NW and nanofin are selected as two representative nanogenerator elements. Their dynamic responses are modeled using a single-degree of freedom system with a series of damping ratios. Combining the transfer functions of mechanical vibration and piezoelectric charge generation, we define the output power and efficiencies as functions of the vibration frequency and the sizes. The optimal size for constructing a high efficiency and high-power nanogenerator is suggested. The material dependence of a dynamic system is also studied based on different piezoelectric and ferroelectric material systems, including ZnO, $BaTiO_3$, and $(1-x)\,Pb(Mg_{1/3}Nb_{2/3})O_3-xPbTiO_3$. This research reveals a comprehensive relationship between the mechanical energy harvesting ability and the nanomaterials' morphologies, dimensions, and properties. It provides a guideline for the design of high-power nanogenerators and the development of piezoelectric nanodevices in general.
 [doi:10.1063/1.3462468]

I. INTRODUCTION

Vibration-based mechanical energy is the most ubiquitous and accessible energy source in the surroundings. Harvesting this type of energy exhibits a great potential for remote/wireless sensing, charging batteries, and powering electronic devices.[1–3] Piezoelectric and ferroelectric materials, such as lead zirconate titanate (PZT), $(1-x)\,Pb(Mg_{1/3}Nb_{2/3})O_3-xPbTiO_3$ (PMN-PT), $BaTiO_3$, ZnO, poly(vinylidene fluoride) (PVDF), etc., have been intensively studied as effective and efficient building blocks for converting ambient mechanical energy into electricity.[4–8] Based on these materials, a variety of micro- or nanoelectromechanical systems (MEMS or NEMS) were developed for harvesting energies from random vibrations, mechanical waves, or body movements like walking, running, or typing.[9–13] Recently, a promising concept has been demonstrated by using piezoelectric ZnO nanowires (NWs) to harvest micro- and nanoscale mechanical energy (the nanogenerator).[14–16] Owing to the small size and high flexibility of the NWs, the nanogenerators are very sensitive to small level mechanical disturbances and are ideal for powering wireless sensors, microrobots, NEMS/MEMS, and bioimplantable devices.[12,17,18] Successful prototypes have been developed using vertically aligned ZnO NWs. Continuous direct-current output was obtained from the nanogenerators driven by ultrasonic waves.[7] A textile fiber based nanogenerator has also been developed for harvesting low-frequency vibration/friction energies.[19]

The primary principle of nanogenerator lies on bending induced piezoelectricity generated on the NW side surfaces. Perturbation theory and finite elements method have been carried out to calculate the electrostatic potential generated in a single bent ZnO NW.[20] This theoretical work is serving as the guidance for estimating the output voltage, power, and efficiency, and for optimizing the design of nanogenerators. However, the information obtained from the static calculation may not be sufficient for all possible situations. For example, vibration of the NW is one typical mechanism of mechanical energy harvesting. The harmonic vibration at the resonant frequency may be triggered under certain circumstance by ambient mechanical vibrations, which usually have a wide frequency spectrum. To optimize the design of nanogenerators and substantially improve the output power, it is essential to understand how the NWs respond mechanically and electrically to different vibration frequencies. Thus, the dynamic properties of piezoelectric NWs become critical for analyzing the energy harvesting behavior of the nanogenerators.

In this paper, we established a general theoretical framework for estimating the potential, output power and energy conversion efficiency of piezoelectric nanostructures. This model was applied to ZnO NWs, ZnO nanofins (NFs),[21] and ferroelectric $BaTiO_3$, PMN-PT single crystal NWs in both static and dynamic fashions. The size related energy harvesting abilities were also predicted. This work would provide comprehensive guidance for the design of high-power nanogenerators, and the development of piezoelectric nanodevices in general.

[a)]Electronic mail: xudong@engr.wisc.edu.

II. THEORETICAL FRAMEWORK

We first present a general theoretical framework that will be used for all piezoelectric materials with all types of morphologies. For a dielectric and piezoelectric material system, when the material is placed in an electric filed and subjected to an external force, the constitutive relations are

$$\begin{cases} \sigma_p = c_{pq}\varepsilon_q - e_{kp}E_k \\ D_i = e_{iq}\varepsilon_q + k_{ik}E_k \end{cases}, \tag{1}$$

where ε_q and σ_p are the strain and stress tensor, respectively. e_{kp}, k_{ik}, and D_i are the linear piezoelectric coefficient, dielectric constant, and electric displacement, respectively. e_{iq} is the transpose of e_{kp}. In order to accurately describe the elastic constitutive behavior of orthotropic piezoelectric materials, six compliance parameters (c_{11}, c_{12}, c_{13}, c_{33}, c_{44}, and c_{66}) are needed to calibrate the elastic constants. To simplify the case, nanostructures with a large aspect ratio can be approximately considered as an isotropic system, where the elastic constants are given by the effective Young's modulus E, shear modulus G, and Poisson's ratio v (Refs. 22 and 23)

$$\begin{cases} E = \dfrac{(A-B+3C)(A+2B)}{2A+3B+C} \\ v = \dfrac{A+4B-2C}{4A+6B+2C} \\ G = \dfrac{E}{2(1+v)} \end{cases}, \quad \text{where} \quad \begin{cases} A = \dfrac{2c_{11}+c_{33}}{3} \\ B = \dfrac{2c_{13}+c_{12}}{3} \\ C = \dfrac{2c_{44}+c_{66}}{3} \end{cases}. \tag{2}$$

It has been found that both the radial and tangential elastic moduli of ZnO NWs become nearly constant when the NWs' radii are larger than 20 nm,[24] which covers the applicable size range of nanogenerator design. Therefore, in our analysis, we simply assume all the elastic constants are size independent. In such a system, the relationship between strain and stress is given by Hooke's law

$$\begin{pmatrix} \varepsilon_1 \\ \varepsilon_2 \\ \varepsilon_3 \\ \varepsilon_4 \\ \varepsilon_5 \\ \varepsilon_6 \end{pmatrix} = \frac{1}{E}\begin{pmatrix} 1 & -v & -v & 0 & 0 & 0 \\ -v & 1 & -v & 0 & 0 & 0 \\ -v & -v & 1 & 0 & 0 & 0 \\ 0 & 0 & 0 & 2(1+v) & 0 & 0 \\ 0 & 0 & 0 & 0 & 2(1+v) & 0 \\ 0 & 0 & 0 & 0 & 0 & 2(1+v) \end{pmatrix}\begin{pmatrix} \sigma_1 \\ \sigma_2 \\ \sigma_3 \\ \sigma_4 \\ \sigma_5 \\ \sigma_6 \end{pmatrix}. \tag{3}$$

In this paper, we split our discussion into three different morphologies: rectangular NW, hexagonal NW, and two-dimensional (2D) NF, which would cover the majority of possible configurations of nanogenerator building blocks. A general condition that was used in our calculation is to assume the nanostructures are perpendicular to the substrate with one end fixed on the surface and the other end freestanding. All the physical coefficients were considered as constants and size and temperature independent.

A. Rectangular NW structure

Most high-performance piezoelectric or ferroelectric materials, such as $BaTiO_3$, PMN-PT, etc., belong to the perovskites, which have a cubic or tetragonal structure. NWs made from these materials typically exhibit a rectangular or square cross section.[25,26] Therefore, we consider the rectangular NW system as the first general case for piezoelectricity calculation. In this system, a square cross section is assumed, and the length and width of the NW are defined as l and b, respectively. In the Cartesian coordinate applied to the NW, the origin of the coordinate is at the center of the bottom surface; the z axis coincides with the centerline of the NW; and the x and y axes are parallel to the two edges of the cross section, respectively. [Fig. 1(a)].

When a lateral continuous force f_y is applied at the free end of the NW and parallel to the y direction, normal stress σ_3 and shear stress components σ_4 and σ_5 appear on the cross section along the z direction; while other three stress components σ_1, σ_2, and σ_6 are zero. Based on the Saint-Venant cantilever beam bending theory for a rectangular beam, the stress components σ_3, σ_4, and σ_5 are given as[27]

$$\begin{cases} \sigma_3 = -\dfrac{f_y}{I_{xx}}y(l-z) \\ \sigma_4 = \dfrac{f_y}{2I_{xx}}\left(y^2 - \dfrac{1}{4}b^2\right)\left[5nx^4 + 3\left(m - \dfrac{1}{4}b^2n\right)x^2 - \dfrac{1}{4}b^2m - 1\right] \\ \sigma_5 = -\dfrac{f_y}{I_{xx}}y\left[nx^5 + \left(m - \dfrac{1}{4}b^2n\right)x^3 - \dfrac{1}{4}b^2mx\right] \end{cases}, \tag{4}$$

where $I_{xx}=(b^4/12)$, is the moment of inertia with respect to the x axis; $m=-(1335/1042)(v/1+v)(1/b^2)$ and $n=-(2310/3647)(v/1+v)(1/b^4)$. When a constant external voltage V_y is applied on the NW along the y direction, a uniform electric field $E_y=V_y/b$ will be induced insider the NW. Therefore, for a general case that both f_y and V_y present, the strain components can be obtained by solving Eqs. (1), (3), and (4)

$$\begin{cases} \varepsilon_3 = -\dfrac{f_y}{EI_{xx}} y(l-z) \\ \varepsilon_4 = \dfrac{f_y(1+v)}{EI_{xx}}\left(y^2 - \dfrac{1}{4}b^2\right)\left[5nx^4 + 3\left(m - \dfrac{1}{4}b^2 n\right)x^2 - \dfrac{1}{4}b^2 m - 1\right] + \dfrac{2(1+v)}{E} e_{15} E_y \\ \varepsilon_5 = -\dfrac{2f_y(1+v)}{EI_{xx}} y\left[nx^5 + \left(m - \dfrac{1}{4}b^2 n\right)x^3 - \dfrac{1}{4}b^2 mx\right] \end{cases} . \tag{5}$$

Thus, the electric displacements D_i are

$$\begin{cases} D_1 = -\dfrac{2f_y(1+v)}{EI_{xx}} e_{15} y\left[nx^5 + \left(m - \dfrac{1}{4}b^2 n\right)x^3 - \dfrac{1}{4}b^2 mx\right] \\ D_2 = \dfrac{f_y(1+v)}{EI_{xx}} e_{15}\left(y^2 - \dfrac{1}{4}b^2\right)\left[5nx^4 + 3\left(m - \dfrac{1}{4}b^2 n\right)x^2 - \dfrac{1}{4}b^2 m - 1\right] + \dfrac{2(1+v)}{E} e_{15}^2 E_y + k_{11} E_y \\ D_3 = \dfrac{f_y}{EI_{xx}}(2v e_{31} - e_{33}) y(l-z) \end{cases} . \tag{6}$$

It should be noted that the elastic boundary conditions of the NW are regarded as "free" except at the fixed end. The overall charge displacement can be used to resolve the coupling effect between mechanical deflection and piezoelectric voltage, where both mechanical and electrical energies were taken into account.[28] Since the electric field is assumed to be applied along the y direction, the electric energy density is: $u_E = (1/2) D_2 E_y$. On the other hand, the elastic energy density associated with the deformation is given by the product of the stress and strain as $u_M = 1/2\ (\sigma_3\varepsilon_3 + \sigma_4\varepsilon_4 + \sigma_5\varepsilon_5)$. Combination of these two parts gives the overall energy density due to the electric field and the mechanical deflection. Thus, the total energy stored in the NW can be obtained by integration over the entire structure

$$\begin{aligned} U_{tot} &= \int_0^L \int_{-b/2}^{b/2} \int_{-b/2}^{b/2} u_{tot} dy dx dz = \int_0^L \int_{-b/2}^{b/2} \int_{-b/2}^{b/2} \left[\frac{1}{2}(\sigma_3\varepsilon_3 + \sigma_4\varepsilon_4 + \sigma_5\varepsilon_5) + \frac{1}{2} D_2 E_y\right] dx dy dz = \frac{f_y(1+v) e_{15} l b^4}{6EI_{xx}} E_y \\ &+ \frac{1}{2}\left[\frac{2(1+v)}{E} e_{15}^2 + k_{11}\right] l b^2 E_y^2 + \frac{1}{2E}\int_0^L \int_{-b/2}^{b/2} \int_{-b/2}^{b/2} [\sigma_3^2 + 2(1+v)(\sigma_4^2 + \sigma_5^2)] dx dy dz. \end{aligned} \tag{7}$$

Equation (7) gives that the total internal energy contains three terms. The first term is the coupled electromechanical energy and reveals how much energy can be converted from mechanical to electrical. The second term is the pure electrical energy, which is corresponding to the electrical displacement due to the existence of electrical field. The last term is the elastic energy induced by mechanical deflection. The first two terms represent the NW's total electric energy, which can be related to the total charge that is stored in the NW via $U_e = \int Q_{tot} dV_y$. For the case of using a rectangular NW as a nanogenerator element, the rectangular NW can be assumed to act as a parallel capacitor with infinitesimally-thick electrodes applied on both side surfaces for outputting the maximum electric energy. Therefore, these two side surfaces would exhibit equal potential but with opposite signs. Thus, the total charge that can be collected by the two side surfaces can be extracted as

$$Q_{tot} = \frac{\partial U_{tot}}{\partial V_y} = \frac{f_y(1+v) b^3 l e_{15}}{6EI_{xx}} + \left[\frac{2(1+v)}{E} e_{15}^2 + k_{11}\right] l V_y. \tag{8}$$

As presented in Eq. (8), the total charge is described in terms of applied force [the first term in Eq. (8)] and external voltage [the second term in Eq. (8)]. The total charge can be used to derive the NW's capacitance along the y direction

$$C_p = \frac{\partial Q_{tot}}{\partial V_y} = \left[\frac{2(1+v)}{E} e_{15}^2 + k_{11}\right] l. \tag{9}$$

For nanogenerator application, no external voltage is applied and the NW can be considered as an open circuit system. Thus, the actual generated charge is only the first term in Eq. (8), which is defined as the piezoelectric charge (Q_p). Knowing the capacitance of the NW from Eq. (9), we can estimate the maximum voltage that can be produced between the two side surfaces of a rectangular piezoelectric NW due to an external force

$$\Delta V_{\max, r\mathrm{NW}} = \frac{Q_p}{C_p} = \frac{f_y(1+v) b^3 e_{15}}{6I_{xx}[2(1+v)e_{15}^2 + k_{11} E]}. \tag{10}$$

B. Hexagonal NW structure

Most NWs with wurtzite structure, such as ZnO, GaN, etc., exhibit a hexagonal cross section. To solve the stress of a hexagonal NW system, the hexagonal cross section can be approximated to an ellipse with negligible errors [as marked by the dashed circle in Fig. 1(b)].[29] To solve the piezoelectric potential, the hexagonal geometry was directly used. In this system, the length and the width of each side of the NW

were defined as l and b, respectively. The same Cartesian coordinate as the rectangular NW system was applied to the hexagonal system [Fig. 1(b)].

When a continuous force f_y was applied at the free end of a hexagonal NW perpendicularly to one side surface, the stress components σ_3, σ_4, and σ_5 are given as[27]

$$\begin{cases} \sigma_3 = -\dfrac{f_y}{I_{xx}} y(l-z) \\ \sigma_4 = \dfrac{f_y}{I_{xx}} \dfrac{11+8v}{30(1+v)} \left[b^2 - y^2 - \dfrac{4-8v}{11+8v} x^2 \right] \\ \sigma_5 = -\dfrac{f_y}{I_{xx}} \dfrac{4+7v}{15(1+v)} xy \end{cases}, \tag{11}$$

where $I_{xx}=(5\sqrt{3}/16)b^4$. By going through the same procedure as the rectangular NW system and still assuming that a uniform electric field $E_y=V_y/\sqrt{3}b$ is applied along the y direction, the electric displacement in a hexagonal NW was derived to be

$$\begin{cases} D_1 = -\dfrac{f_y}{I_{xx}E} \dfrac{8+14v}{15} e_{15} xy \\ D_2 = \dfrac{f_y}{I_{xx}E} \dfrac{11+8v}{15} e_{15} \left(b^2 - y^2 - \dfrac{4-8v}{11+8v} x^2 \right) + \dfrac{2(1+v)}{E} e_{15}^2 E_y + k_{11} E_y \\ D_3 = \dfrac{f_y}{I_{xx}E} (2v e_{31} - e_{33}) y(l-z) \end{cases}. \tag{12}$$

On a hexagonal NW, in order to output the highest piezoelectric potential, two imaginary electrodes were assumed to cover only the two side surfaces that are perpendicular to the y direction. It is because the piezoelectric potential drops quickly along the four neighboring side surfaces. Covering them with the imaginary electrode to create an equal potential surface for outputting charge will lower the overall output potential. Thus, in this case, the effective NW volume which contributes to piezoelectric charge is the rectangular portion in-between the two electrodes. Therefore, the same method as for the rectangular NW system was used to estimate the charge generated by the piezoelectric effect (Q_p), the effective capacitance (C_p) and the highest piezoelectric voltage difference across the body of a hexagonal NW was then obtained as

$$\begin{cases} Q_{tot} = \dfrac{f_y}{36 I_{xx} E} b^3 l e_{15} (19+16v) + \dfrac{\sqrt{3}}{3} \left[\dfrac{2(1+v)}{E} e_{15}^2 + k_{11} \right] l V_y \\ C_p = \dfrac{\sqrt{3}}{3} \left[\dfrac{2(1+v)}{E} e_{15}^2 + k_{11} \right] l \\ \Delta V_{\max,h\mathrm{NW}} = \dfrac{\sqrt{3} F_y (19+16v) b^3 e_{15}}{36 I_{xx} [2(1+v) e_{15}^2 + k_{11} E]} \end{cases}. \tag{13}$$

C. 2D NF structure

Vertical 2D thinfilms (the NFs) have been suggested as one promising building block for the nanogenerator, since they can be considered as lines of NWs that are fused together, which would potentially solve the integration challenge of nanogenerator design.[30] Based on the same method, the equation for estimating the voltage of such a structure was derived. A typical NF structure is assumed to have a rectangular cross section, where the width (b) is much larger than the thickness (t). The height of the NF is defined as h [Fig. 1(c)]. To bend a NF structure, a lateral force f_y is assumed to be applied along the thickness direction (the y direction) and uniformly distributed along the width direction (the x direction) at its free end so that the strain in the NF is only a function of y. Meanwhile, a constant external electric field $E_y=V_y/t$ is also assumed to be applied along the y direction. Thus, the stresses and electric displacements of the NF are given by[27]

$$\begin{cases} \sigma_3 = -\dfrac{f_y}{I_{xx}} y(h-z) \\ \sigma_4 = \dfrac{1}{(1+v)} \dfrac{f_y}{2I_{xx}} \left(\dfrac{t^2}{4} - y^2 \right) \\ \sigma_5 = -\dfrac{v}{1+v} \dfrac{f_y}{I_{xx}} xy \end{cases} \tag{14}$$

and

$$\begin{cases} D_1 = -\dfrac{2 f_y v}{E I_{xx}} xy e_{15} \\ D_2 = \dfrac{f_y}{I_{xx}E} \left(\dfrac{t^2}{4} - y^2 \right) e_{15} + \dfrac{2(1+v)}{E} e_{15}^2 E_y + k_{11} E_y \\ D_3 = \dfrac{f_y}{I_{xx}E} (2v e_{31} - e_{33}) y(h-z) \end{cases}, \tag{15}$$

respectively, where $I_{xx}=bt^3/12$. To calculate the maximum piezoelectric voltage between the two side surfaces, the same method was applied to obtain the generated charge, the capacitance and the generated maximum voltage between the two electrodes. The final results are given by the following equations:

$$\begin{cases} Q_{tot} = \dfrac{f_y b t^2 l e^{15}}{6 E I_{xx}} + \left[\dfrac{2(1+v)}{E} e_{15}^2 + k_{11} \right] bl \dfrac{V_y}{t} \\ C = \left[\dfrac{2(1+v)}{E} e_{15}^2 + k_{11} \right] bl \dfrac{1}{t} \\ \Delta V_{\max,\mathrm{NF}} = \dfrac{f_y t^3 e_{15}}{6 I_{xx} [2(1+v) e_{15}^2 + k_{11} E]} \end{cases}. \tag{16}$$

III. STATIC ANALYSIS

The voltage-to-force relations of different morphologies were first used to analyze the maximum piezoelectric potential that can be generated by typical piezoelectric and ferroelectric nanomaterials when they are deflected under a constant external force. Here, $BaTiO_3$ NW (square cross section was assumed), ZnO NW (hexagonal morphology was assumed), and ZnO NF were selected to represent the three different morphologies. Physical parameters of ZnO and $BaTiO_3$ that were used in the potential calculation were collected from other references and listed in Table I.[31–34] Both ZnO and $BaTiO_3$ in this analysis were considered as a perfect dielectric medium with negligible free charge carrier density. The maximum piezoelectric potentials were plotted

TABLE I. Dielectric constants that were used in the theoretical piezoelectric potential calculation.

	Elastic stiffness constant (GPa)						Density (kg/m^3)	Electrical resistivity (Ω m)	k_{11}	e_{15} (C/m^2)
	c_{11}	c_{12}	c_{13}	c_{33}	c_{44}	c_{66}				
ZnO	209.7	121.1	105.1	210.9	42.47	44.29	5606	3.5×10^8	7.77	−0.45
$BaTiO_3$	222	108	111	151	61	134	6012	$>1\times10^{11}$	4400	34.2
PMN-PT	160.4	149.6	75.1	120	53.8	28.7	8093	$>1\times10^{11}$	7093	31.84

as functions of the external force and their dimensions following Eqs. (10), (13), and (16), as shown in the insets of Figs. 1(d)–1(f) for $BaTiO_3$ NW, ZnO NW, and ZnO NF, respectively. In general, their maximum potential is proportional to the external force and inversely proportional to the thickness or width but not related to their length. Theoretically, high piezoelectric potential would be generated when a large external force is applied onto a NW with a small thickness, because large deflection is produced. However, in real cases, the deflection of nanostructures is restricted by their mechanical strength and flexibility, thus, the highest potentials plotted in the insets of Figs. 1(d)–1(f) are practically impossible. In order to reveal the achievable piezoelectric potentials by nanostructures, we calculated and superimposed the mechanical limitation boundaries into the potential plots.

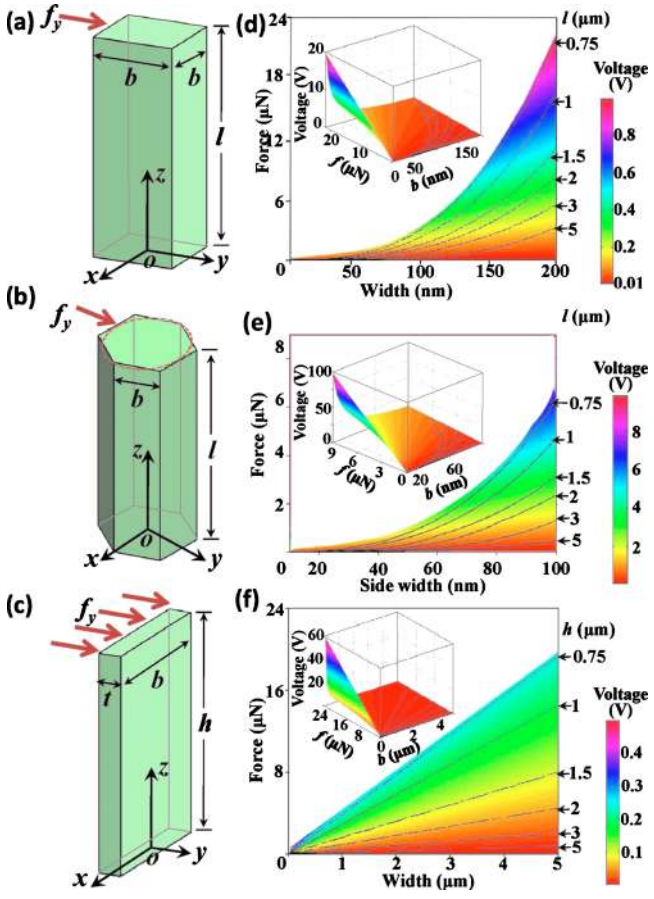

FIG. 1. (Color online) Schematic structures and the coordinate systems of (a) a rectangular NW; (b) a hexagonal NW; and (c) a 2D NF. The static analysis of the maximum allowable piezoelectric potential that can be generated by (d) a $BaTiO_3$ NW; (e) a ZnO NW; and (f) a ZnO NF at different heights. Insets are the corresponding full range plots of the piezoelectric potential to the force and size relationships.

The mechanical limitation boundaries were established based on two criteria—the maximum strain and deflection angle. It has been found that NWs can sustain much higher strains comparing to their bulk form. Elastic deformation has been discovered on ZnO NWs with a strain up to ~7.7%.[35] Unfortunately, such data for $BaTiO_3$ NWs are currently unavailable. Therefore, we assume all the three nanostructures that are studied in this paper can sustain a maximum strain of 7.0%. On the other hand, thin NWs can reach fairly large deflection angles before maximizing their strain, whereas the stain evaluation is based on the small-angle approximation and may not be valid at large deflection angles. Large deflection angles are also not desired for electrical energy collection. Therefore, we define ±30° to be the maximum deflection angle of the nanostructure during mechanical energy harvesting.

The mechanical limitation boundaries of nanostructures [dark lines in the insets of Figs. 1(d)–1(f)] were calculated at 7.0% strain and ±30° deflection angle, whichever was reached first. For a nanostructure, apparently, σ_3 is larger than σ_4 and σ_5 by comparing the equations in Eqs. (4), (11), and (14). Reproducing the equation of σ_3, the applied force will be

$$f_y = \frac{3EI_{xx}s}{l^3}, \tag{17}$$

where s is the deflection of the nanostructure. When y and z are equal to $-b/2$ and 0, the maximum stress is found to be

$$\sigma_{\max} = \frac{3Ebs}{2l^2} \tag{18}$$

where b is the width or thickness of the nanostructure. Then, we have

$$\varepsilon_{\max} = \frac{3bs}{2l^2} = \frac{3b\tan\theta}{2l}, \tag{19}$$

where θ is the deflection angle of the nanostructure.

Based on the mechanical boundary condition, forces larger than a critical value could either damage or over deflect the nanostructure (larger than 30°). To find the critical values of the forces, a critical dimension b_{critical} is defined. From $\varepsilon_{\max}$, we have

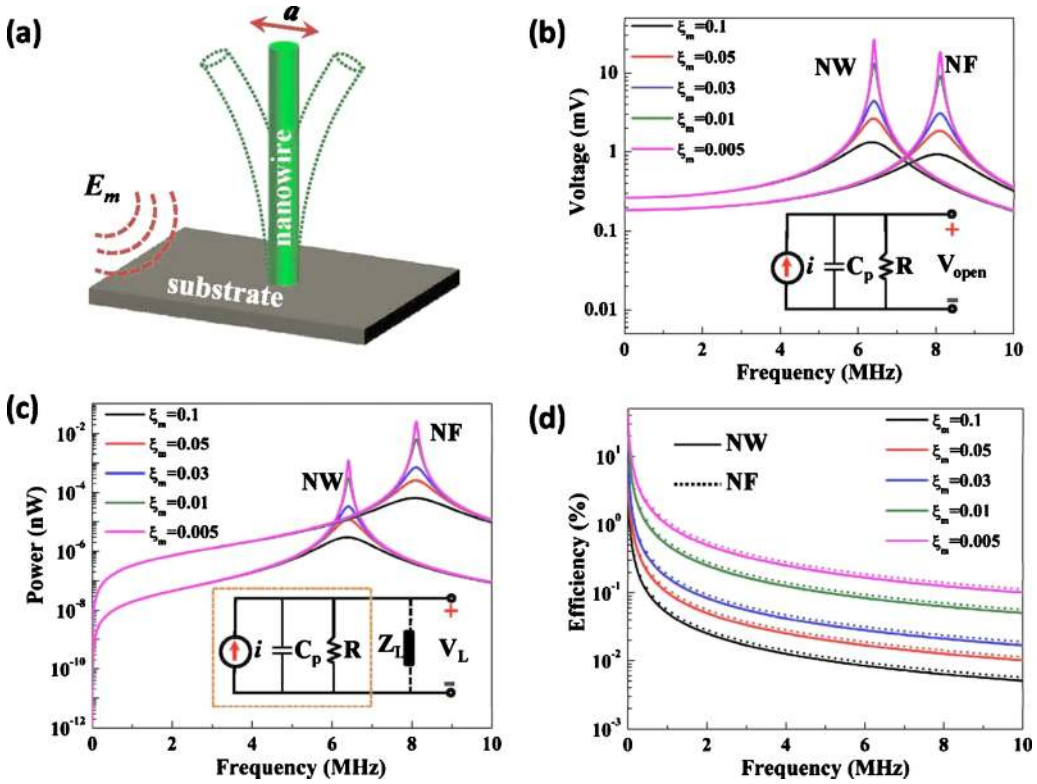

FIG. 2. (Color online) Morphology related power generation ability analysis. (a) A schematic illustration of a dynamic analysis model, where the NW is agitated into vibration by an external vibration mechanical energy applied through the substrate; (b) the open circuit voltage; (c) the output power; and (d) the energy conversion efficiency of a ZnO NW and a ZnO NF structure under different damping ratios. Insets of (b) and (c) are the equivalent circuit of the nanostructure component.

$$b = \frac{2l\varepsilon_{\max}}{3\tan\theta}. \tag{20}$$

We define

$$b_{\text{critical}} = \frac{2l\varepsilon_{\text{fracture}}}{3\tan 30^\circ}, \tag{21}$$

with a certain length of nanostructure, when b is smaller than b_{critical}, the critical force is

$$f_{\text{critical}} = \frac{3EI_{xx}\tan 30^\circ}{l^3}. \tag{22}$$

When the width or the thickness of the nanostructure is smaller than the critical value, the nanostructure reaches its maximum deflection angle but the maximum strain is smaller than the fracture strain. When b is larger than b_{critical}, the critical force is

$$f_{\text{critical}} = \frac{3EI_{xx}\tan\theta}{l^3}, \tag{23}$$

where $\tan\theta$ is equal to $2l\varepsilon_{\text{fracture}}/3b$ This describes the situation when the nanostructure reaches its maximum strain but the deflection angle is smaller than 30°.

The boundary lines for NWs and NFs with various heights were determined and the allowable potential distributions inside the boundary lines are shown in Figs. 1(d)–1(f) with different lengths or heights: 0.75, 1, 1.5, 2, 3, and 5 μm. Comparing $BaTiO_3$ and ZnO NWs with the same size and under the same force, ZnO exhibits much higher piezoelectric potential, although its piezoelectric coefficient is much smaller than that of $BaTiO_3$. The reason for $BaTiO_3$ NWs to show lower potential could be attributed to their much larger dielectric constant, which leads to a large capacitance. It is known that the piezoelectric effect directly induces charge and the piezoelectric potential is derived from the amount of charge via the relation $V=Q/C_p$. Therefore, significantly larger dielectric constant of $BaTiO_3$ would induce a lower effective voltage appearing along the NW surface. Besides, the piezoelectric potential of ZnO was also overestimated because the free charge effect was not considered in this analysis.[36] Nevertheless, this plot presents a close result comparing to that calculated by Gao and Wang[20] via electrodynamics method. A much larger force is needed for a ZnO NF to generate the same voltage due to the enlarged size. However, higher output power can be expected from the NF structure since the current output is enhanced.

IV. DYNAMIC ANALYSIS

The first independently operated nanogenerator prototype is designed to be driven by ultrasonic waves. In fact, stimulating a piezoelectric beam into vibration has been broadly used for harvesting mechanical energy in most MEMS devices. Therefore, to quantitatively understand the dynamic responses of a piezoelectric NW under vibration is essential for the development of practical nanogenerator systems. The system used for our dynamic analysis is schematically shown in Fig. 2(a). Same as the static conditions, the nanostructure (NW or NF) was assumed to have its bottom

end fixed on the substrate and the other end to be free. An external mechanical energy in a wave form is applied through the substrate and agitates the vibration of the NW at the same frequency. We also assume the external mechanical energy is continuous, constant, and sufficiently large. The vibration of the NW is described by its acceleration $a(t)$, which can be converted into the force applied to the NWs tip by Newton's Law: $f(t)=m^*a(t)$, where m^* is the effective mass of the vibration beam and can be approximated as one-third of the NWs mass.[37] Such a vibration causes the piezoelectric device a flexural vibration and alternating electrical charges will be generated along the two side surfaces of the NW through the direct piezoelectric effect. Considering each NW as a single-degree of freedom system, the motion of the NW under vibration can be written as[37]

$$m^*\ddot{y}(t)+D\dot{y}(t)+Ky(t)=f(t)=m^*a(t), \tag{24}$$

where $K=3EI/l^3$ is the spring constant of the system, $D=2m^*\zeta\omega_n$ is viscous damping coefficient, $\omega_n=\sqrt{K/m^*}$ is the natural frequency of the nanostructure, and ζ is the damping ratio. Equation (24) can be written in the Laplace domain by setting the initial conditions equal to zero

$$m^*s^2Y+DsY+KY=m^*a(s), \tag{25}$$

where $s=j\omega$. Thus, the deflection at the free end of the NW is

$$Y(s)=\frac{a(s)}{s^2+2\zeta\omega_n s+\omega_n^2}. \tag{26}$$

Therefore, the generated charge by the nanogenerator due to the deflection can be obtained in the frequency domain as

$$Q(s)=K_q\frac{a(s)}{s^2+2\zeta\omega_n s+\omega_n^2}, \tag{27}$$

where K_q is the charge generation per unit deflection (C/m), which equals to the static piezoelectric charge Q_p divided by the maximum deflection y_{max} induced by external force f_y. For the application as a power source, each piezoelectric nanostructure component can be regarded as a current source with a capacitance C_p and a leakage resistance R, as shown in the inset of Figs. 2(b) and 2(c).

To analyze the power generation performance of each nanostructure, a load resistance $Z_L=1/\omega C_p$ is connected to the nanogenerator [inset of Fig. 2(c)] for the extraction of maximum electrical power output.[38] Applying the Kirchhoff s laws to the equivalent circuit, the generated voltage applied on the external load can be obtained by

$$V(s)=\frac{m^*aK_q}{C_pK}\frac{\omega_n^2}{s^2+2\zeta\omega_n s+\omega_n^2}\frac{\tau s}{\omega\tau+\tau s+1}, \tag{28}$$

where $\tau=RC_p$ is the time constant, ω is the angular velocity of the applied force. If the load resistance Z_L is infinitely large, Eq. (28) becomes the open circuit voltage. Therefore, by using the equations derived in the static case to recover K_q and C_p, the generated open circuit voltage of rectangular NWs, hexagonal NWs, and 2D NFs can be obtained as

$$\begin{cases} V_{r\mathrm{NW}}=\dfrac{m^*a(1+v)b^3e_{15}}{6I_{xx}[2(1+v)e_{15}^2+k_{11}E]}\dfrac{\omega_n^2}{s^2+2\zeta\omega_n s+\omega_n^2}\dfrac{\tau s}{\tau s+1} \\ V_{h\mathrm{NW}}=\dfrac{\sqrt{3}m^*a(19+16v)b^3e_{15}}{36I_{xx}[2(1+v)e_{15}^2+k_{11}E]}\dfrac{\omega_n^2}{s^2+2\zeta\omega_n s+\omega_n^2}\dfrac{\tau s}{\tau s+1} \\ V_{\mathrm{NF}}=\dfrac{m^*at^3e_{15}}{6I_{xx}[2(1+v)e_{15}^2+k_{11}E]}\dfrac{\omega_n^2}{s^2+2\zeta\omega_n s+\omega_n^2}\dfrac{\tau s}{\tau s+1} \end{cases}. \tag{29}$$

The electrical power extracted by the load Z_L is considered as the practical output power of these morphologies, which can be derived from Eq. (29) via the relation $P=V^2/Z_L$.

$$\begin{cases} P_{r\mathrm{NW}}=\dfrac{m^{*2}a^2b^6le_{15}^2(1+v)^2}{36I_{xx}^2E[2(1+v)e_{15}^2+k_{11}E]}\dfrac{\omega_n^4}{(s^2+2\zeta\omega_n s+\omega_n^2)^2}\dfrac{\omega s^2\tau^2}{(\omega\tau+s\tau+1)^2} \\ P_{h\mathrm{NW}}=\dfrac{\sqrt{3}m^{*2}a^2b^6le_{15}^2(19+16v)^2}{1296I_{xx}^2E[2(1+v)e_{15}^2+k_{11}E]}\dfrac{\omega_n^4}{(s^2+2\zeta\omega_n s+\omega_n^2)^2}\dfrac{\omega s^2\tau^2}{(\omega\tau+s\tau+1)^2} \\ P_{\mathrm{NF}}=\dfrac{m^{*2}a^2t^5bHe_{15}^2}{36I_{xx}^2E[2(1+v)e_{15}^2+k_{11}E]}\dfrac{\omega_n^4}{(s^2+2\zeta\omega_n s+\omega_n^2)^2}\dfrac{\omega s^2\tau^2}{(\omega\tau+s\tau+1)^2} \end{cases}. \tag{30}$$

In order to define the energy conversion efficiency, the input mechanical power needs to be quantified. In a real situation, it is reasonable to assume that the mechanical energy in the surroundings is "infinite" for supporting the operation of nanogenerators. Thus, the frequency and amplitude of the input mechanical wave can be regarded as constants. Therefore, the input mechanical power P_{in} can be considered as the energy that is absorbed by the nanostructure to overcome the damping and sustain its vibration. In such a system, the damping of mechanical energy consists of two aspects: P_e, the power dissipated due to electrical consumption represented by damping ratio ζ_e; and P_m, the power dissipated due to mechanical damping represented by damping ratio ζ_m. The electrical power dissipation includes the output power P_{out}

that is consumed by the external load and the power consumed by the inherent impedance of the piezoelectric nanostructure. In an ideal situation when the load resistance equals to $1/\omega C_p$, the internal power dissipation is approximately equal to P_{out}. For a cantilever beam system, the power dissipated due to mechanical damping is[37]

$$P_m = 2\pi\zeta_m\sqrt{Km^*}\omega Y^2/(2\pi/\omega) = \zeta_m m^*\omega_n\omega^2 a^2 \frac{1}{(s^2+2\zeta\omega_n s+\omega_n^2)^2}. \tag{31}$$

Thus, the ratio between the output electric power and input mechanical power gives the energy conversion efficiency of the nanostructure for converting mechanical energy into usable electric energy: $\eta = P_{\text{out}}/P_{\text{in}} = P_{\text{out}}/(2P_{\text{out}}+P_m)$. For the three different morphologies, the efficiencies are presented by the following equations:

$$\begin{cases} \eta_{r\text{NW}} = \dfrac{m^*(1+v)^2 b^6 l e_{15}^2 s^2\tau^2\omega_n^3}{2m^*(1+v)^2 b^6 l e_{15}^2 s^2\tau^2\omega_n^3 + 36\zeta_m I_{xx}^2 E[2(1+v)e_{15}^2 + k_{11}E]\omega(\omega\tau+s\tau+1)^2} \\ \eta_{h\text{NW}} = \dfrac{\sqrt{3}m^* b^6 e_{15}^2 l(19+16v)^2 s^2\tau^2\omega_n^3}{2\sqrt{3}m^* b^6 e_{15}^2 l(19+16v)^2 s^2\tau^2\omega_n^3 + 1296\zeta_m I_{xx}^2 E[2(1+v)e_{15}^2 + k_{11}E]\omega(\omega\tau+s\tau+1)^2} \\ \eta_{\text{NF}} = \dfrac{m^* t^5 b H e_{15}^2 s^2\tau^2\omega_n^3}{2m^* t^5 b H e_{15}^2 s^2\tau^2\omega_n^3 + 36\zeta_m I_{xx}^2 E[2(1+v)e_{15}^2 + k_{11}E]\omega(\omega\tau+s\tau+1)^2} \end{cases}. \tag{32}$$

From the efficiency, the total damping ratio of the nanogenerators can be derived by $\zeta = \zeta_e + \zeta_m = \zeta_m/(1-2\eta)$,[39] when the mechanical damping is defined. Equations (29), (30), and (32) present the general expressions of piezoelectric voltage, output power, and energy conversion efficiency for rectangular NWs, hexagonal NWs, and 2D NFs. To plug them in with the physical properties of specific materials and conditions, the power generation ability of different types of nanomaterials can be predicted.

First, these equations were used to illustrate the performance of nanogenerators built upon different nanostructure morphologies (NW and NF). In order to present a reasonable comparison, NW and NF made from the same ZnO material were selected using the physical constants listed in Table I. We also arbitrarily chose five different mechanical damping ratios of 0.005, 0.01, 0.03, 0.05, and 0.1 in our calculation. The same acceleration for the vibration was assumed to be 1×10^7 m/s^2, which results an applied force of 0.0607 nN for ZnO NW ($b=25$ nm, $l=2$ μm) and 1.869 nN for ZnO NF ($t=50$ nm, $l=2$ μm, $b=1$ μm) based on their mechanical properties. Figures 2(b)–2(d) show the generated open circuit voltages, output powers, and efficiencies of a ZnO NW and a ZnO NF as functions of their vibration frequencies under different damping ratios. The piezoelectric voltage and power maximize at the resonant frequency of the nanostructure; while the energy conversion efficiency slowly decays with the increasing of vibration frequency. It is also obvious that the damping ratio has large influences on the amplitudes of these three characteristics. Specifically, the ZnO NW resonates at 6.41 MHz with a maximum open circuit voltage of 26.4 mV and a maximum output power of 1.18×10^{-3} nW, which corresponds to an energy conversion efficiency of ~0.157%. The ZnO NF has a higher resonant frequency at 8.11 MHz and exhibits a lower maximum open circuit voltage of 18.4 mV but higher output power of 0.025 nW with an energy conversion efficiency of ~0.138%. The lower voltage of the NF is resulted from the smaller dynamic deflection under the same acceleration. Its higher output power can be attributed to the much larger surface area, which contributes higher current. The NW shows a little lower energy conversion efficiency than the NF at any damping ratios, because only portion of a hexagonal NW would contribute to the piezoelectric potential due to practical electrodes design. Therefore, without any loss of energy conversion capability, using 2D NFs instead of 1D NWs would improve the assembly accuracy and substantially increase the number of active components in practical nanogenerator devices so as to improve the power output.

The performance of the NW and NF was further evaluated as functions of their sizes. In order to reveal the size dependence of the output power and efficiency, we assumed that the NW and NF are both agitated into vibration at their resonant frequencies with a fixed mechanical damping ratio of 0.005. From Eqs. (30) and (32), the power and efficiency were calculated at different lengths and thicknesses. The plots of these relationships for $BaTiO_3$ NW, ZnO NW, and ZnO NF are shown in Figs. 3(a)–3(c), respectively. Two general conclusions can be drawn from the plots regardless of the morphology and material. First, the output power increases with the increasing of the volume of the nanostructures. This agrees with the property of regular piezoelectric bulk materials—more volume brings more piezoelectric power. Second, the energy conversion efficiency at the resonant frequency increases rapidly with the reducing of the nanostructure's aspect ratio. This suggests that high energy conversion efficiency would be found in a thin-film-like morphology, which is resulted from the faster decay of the mechanical damping energy comparing to the electric output energy when the aspect ratio decreases. The different tracks of the output energy and efficiency indicate the existence of

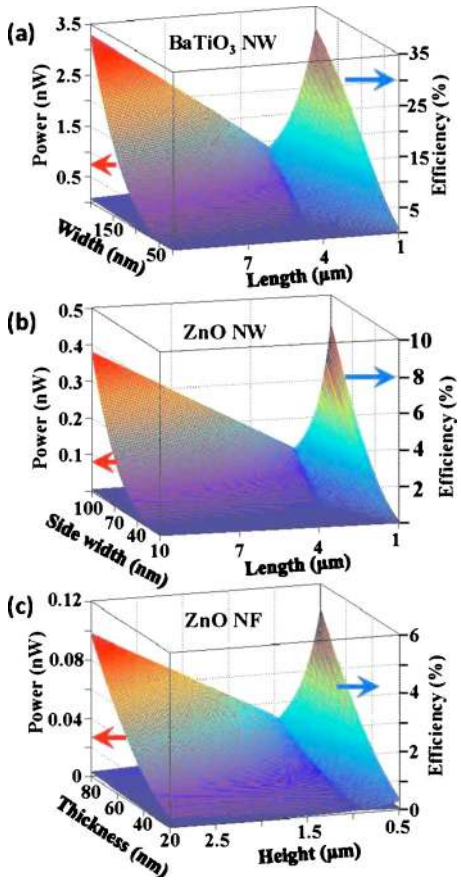

FIG. 3. (Color online) Size related power generation ability analysis. (a) The output power and energy conversion efficiency of $BaTiO_3$ NWs at their resonant frequencies as functions of their length and thickness. (b) The output power and energy conversion efficiency of ZnO NWs at their resonant frequencies as functions of their length and side widths. (c) The output power and energy conversion efficiency of ZnO NFs at their resonant frequencies as functions of their height and thickness.

an optimal size range, where the nanostructures will output reasonable power with reasonable efficiency. Such a size range can be identified from the plots where the power surface intersects with the efficiency surface. For $BaTiO_3$ NWs, their lengths should be 4–5 μm and width should be larger than 100 nm. For ZnO NWs, their lengths should be 3–4 μm and side widths should be larger than 50 nm. For ZnO NFs, their ideal heights are ~1 μm and thicknesses are at least larger than 40 nm. It should be noted that these predictions were established based on the assumption that the ambient mechanical energy is always sufficient. Although the plots show a continuous increasing tendency of both the power and efficiency with the increase in radius or thickness, too large size would need a significantly high external mechanical energy to drive the vibration. Under this condition, the assumption of unlimited mechanical energy will not apply and the solution is beyond the capability of this method.

To study the material dependency of the nanogenerator performance, our model was applied to NWs made from three representative piezoelectric materials. They were ZnO, $BaTiO_3$, and PMN-PT, where we assumed ZnO has a hexagonal morphology and $BaTiO_3$ and PMN-PT have a square cross section. All of them have the same dimension (2 μm long and 50 nm thick) and are driven by the same acceleration of 1×10^7 m/s^2, which results in an applied force of 0.0607 nN for ZnO NW, 0.1 nN for $BaTiO_3$ NW, and 0.1349 nN for PMN-PT NW. A mechanical damping ratio of 0.005 was applied to each case. Under these conditions, their open circuit voltages, output powers, and energy conversion efficiencies were calculated as functions of their vibration frequencies using the constants listed in Table I (Fig. 4). Similar to the static analysis, ZnO NW shows the highest open circuit voltage due to its small dielectric constant, although it has the lowest piezoelectric coefficient [Fig. 4(a)]. At its resonant frequency, ZnO NW generates a voltage of ~26.4 mV, which is ~11–16 times higher than that of PMN-PT and $BaTiO_3$ NWs with the same size. However, both PMN-PT and $BaTiO_3$ NWs exhibit ~8–17 times higher output power and energy conversion efficiency comparing to ZnO NWs [Figs. 4(b) and 4(c)]. This is because both $BaTiO_3$

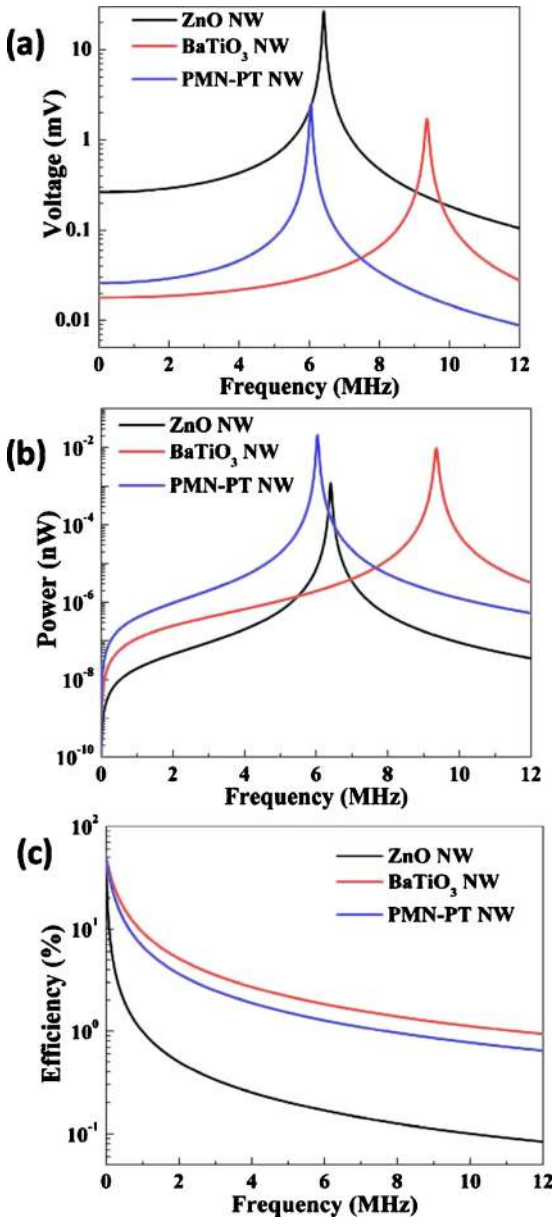

FIG. 4. (Color online) Material related power generation ability analysis. (a) The open circuit voltage; (b) the output power; and (c) the energy conversion efficiency of the same sized NWs made from ZnO, $BaTiO_3$ and PMN-PT.

and PMN-PT have high dielectric constants, which leads to high intrinsic capacitance (C_p). Thus, they only need a small external resistant load ($Z_L = 1/\omega C_p$) to extract the power out from themselves. Therefore, higher output power and higher efficiency are resulted. The highest output power was found from PNM-PT NW at ~0.02 nW with an efficiency of 1.3%. This result suggested that ferroelectric materials, such as $BaTiO_3$ and PMN-PT, could show better performance than ZnO as a power source, while ZnO might be a better choice as a voltage source.

The results in this analysis indicate that piezoelectric nanostructures can generate enough electric energy to power a nanosensor or NEMS systems.[40–42] One major advantage to use NWs instead of bulk materials is the much higher strain that can be sustained by NWs. For instance, the maximum strain for ZnO NW is ~7.7%,[35] while the maximum strain for bulk ZnO material is ~0.2%.[43] Therefore, much higher output power can be expected from nanosized structures comparing to their bulk form. The higher flexibility and strain tolerance of nanostructures could also effectively reduce the risk of potential fracture or damage of the piezoelectric materials under high-frequency vibration conditions, thus, broaden their safety vibration frequency and amplitude range. Within the safety acceleration range, the maximum output power density of bulk PZT, PVDF, and microfiber composite based devices are 1, 0.5 and 0.2 W/cm^3, respectively.[44] While our calculation shows that the ZnO NW, NF, and $BaTiO_3$, PMN-PT NWs would ideally produce as high as 1055 W/cm^3, 2250 W/cm^3, 3×10^4 W/cm^3, and 1.18×10^4 W/cm^3, respectively, assuming the entire space is filled by NWs. These output data indicate that piezoelectric NWs could be superior candidates for mechanical energy harvesting.

V. CONCLUSION

In summary, a general theoretical framework was established for estimating the piezoelectric potential, the output power and the energy conversion efficiency of a series of nanostructures with different morphologies and made from different materials. The static analysis revealed the maximum piezoelectric potential that can be produced by a $BaTiO_3$ NW, a ZnO NW, and a ZnO NF. This analysis will provide us the first principle information to understand the mechanical energy harvesting capability of those materials. Dynamic analyses were conducted to study the power generation ability via the vibration of these nanostructures when ambient vibration energy is absorbed. Systematic comparisons were established between NW and NF morphologies and among ZnO, $BaTiO_3$, and PMN-PN materials by revealing their output voltages, powers, and conversion efficiencies. The size dependency analysis suggested the optimal size choices for NW and NF structures. The highest voltage output was found from ZnO NWs, whereas $BaTiO_3$ and PMN-PT could generate larger output power. The analysis showed that NW morphology would be superior candidates than the bulk forms in mechanical energy harvesting due to their high strain tolerance. This research could serve as a valuable guideline for designing and improving the nanogenerator devices toward an applicable power source.

ACKNOWLEDGMENTS

This work was supported by the National Science Foundation under Grant No. DMR-0905914.

[1] S. Roundy and P. K. Wright, Smart Mater. Struct. **13**, 1131 (2004).
[2] H. A. Sodano, D. J. Inman, and G. Park, J. Intell. Mater. Syst. Struct. **16**, 799 (2005).
[3] G. Poulin, E. Sarraute, and F. Costa, Sens. Actuators, A **116**, 461 (2004).
[4] S. R. Anton and H. A. Sodano, Smart Mater. Struct. **16**, R1 (2007).
[5] C. L. Sun, L. F. Qin, F. Li, and Q. M. Wang, J. Intell. Mater. Syst. Struct. **20**, 559 (2009).
[6] Z. Y. Wang, J. Hu, A. P. Suryavanshi, K. Yum, and M. F. Yu, Nano Lett. **7**, 2966 (2007).
[7] X. D. Wang, J. H. Song, J. Liu, and Z. L. Wang, Science **316**, 102 (2007).
[8] E. Klimiec, W. Zaraska, K. Zaraska, K. P. Gasiorski, T. Sadowski, and M. Pajda, Microelectron. Reliab. **48**, 897 (2008).
[9] J. M. Donelan, Q. Li, V. Naing, J. A. Hoffer, D. J. Weber, and A. D. Kuo, Science **319**, 807 (2008).
[10] A. D. Kuo, Science **309**, 1686 (2005).
[11] L. Mateu and F. Moll, J. Intell. Mater. Syst. Struct. **16**, 835 (2005).
[12] R. Yang, Y. Qin, C. Li, G. Zhu, and Z. L. Wang, Nano Lett. **9**, 1201 (2009).
[13] J. Granstrom, J. Feenstra, H. A. Sodano, and K. Farinholt, Smart Mater. Struct. **16**, 1810 (2007).
[14] Z. L. Wang and J. H. Song, Science **312**, 242 (2006).
[15] R. S. Yang, Y. Qin, L. M. Dai, and Z. L. Wang, Nat. Nanotechnol. **4**, 34 (2009).
[16] S. S. Lin, J. H. Song, Y. F. Lu, and Z. L. Wang, Nanotechnology **20**, 365703 (2009).
[17] X. D. Wang, J. Liu, J. H. Song, and Z. L. Wang, Nano Lett. **7**, 2475 (2007).
[18] Z. L. Wang, Sci. Am. **298**, 82 (2008).
[19] Y. Qin, X. D. Wang, and Z. L. Wang, Nature (London) **451**, 809 (2008).
[20] Y. Gao and Z. L. Wang, Nano Lett. **7**, 2499 (2007).
[21] J. Shi, S. Grutzik, and X. D. Wang, ACS Nano **3**, 1594 (2009).
[22] J. M. J. den Toonder, J. A. W. van Dommelen, and F. P. T. Baaijens, Modell. Simul. Mater. Sci. Eng. **7**, 909 (1999).
[23] R. D. Cook and W. C. Young, *Advanced Mechanics of Materials* (Macmillan, New York, 1985).
[24] G. Stan, C. V. Ciobanu, P. M. Parthangal, and R. F. Cook, Nano Lett. **7**, 3691 (2007).
[25] J. J. Urban, W. S. Yun, Q. Gu, and H. Park, J. Am. Chem. Soc. **124**, 1186 (2002).
[26] Y. Mao, S. Banerjee, and S. S. Wong, J. Am. Chem. Soc. **125**, 15718 (2003).
[27] S. Timoshenko and J. N. Goodier, *Theory of Elasticity*, 3rd ed. (McGraw-Hill, New York, 1969).
[28] B. Aronov, J. Acoust. Soc. Am. **113**, 2638 (2003).
[29] A. Fedotov, *BNL/SNS TECHNICAL NOTE*; *Vol. No. 078* (2000).
[30] C. Falconi, G. Mantinia, A. D'Amico, and Z. L. Wang, Sens. Actuators B **139**, 511 (2009).
[31] J. Peng, H. S. Luo, T. H. He, H. Q. Xu, and D. Lin, Mater. Lett. **59**, 640 (2005).
[32] H. Kind, H. Q. Yan, B. Messer, M. Law, and P. D. Yang, Adv. Mater. (Weinheim, Ger.) **14**, 158 (2002).
[33] M. Zgonik, P. Bernasconi, M. Duelli, R. Schlesser, P. Gunter, M. H. Garrett, D. Rytz, Y. Zhu, and X. Wu, Phys. Rev. B **50**, 5941 (1994).
[34] U. Ozgur, Ya. I. Alivov, C. Liu, A. Teke, M. A. Reshchikov, S. Dogan, V. Avrutin, S.-J. Cho, and H. Morkoc, J. Appl. Phys. **98**, 041301 (2005).
[35] S. Hoffmann, F. Östlund, J. Michler, H. J. Fan, M. Zacharias, S. H. Christiansen, and C. Ballif, Nanotechnology **18**, 205503 (2007).
[36] Y. Gao and Z. L. Wang, Nano Lett. **9**, 1103 (2009).

[37]W. T. Thomson, *Theory of Vibration with Applications*, 3rd ed. (Prentice-Hall, Englewood Cliffs, NJ, 1988).
[38]S. N. Jiang, X. F. Li, S. H. Guo, Y. T. Hu, J. S. Yang, and Q. Jiang, Smart Mater. Struct. **14**, 769 (2005).
[39]Y. C. Shu and I. C. Lien, J. Micromech. Microeng. **16**, 2429 (2006).
[40]J. A. Paradiso and T. Starner, IEEE Pervasive Comput. **4**, 18 (2005).
[41]C. M. Lieber and Z. L. Wang, MRS Bull. **32**, 99 (2007).
[42]B. Z. Tian, X. L. Zheng, T. J. Kempa, Y. Fang, N. F. Yu, G. H. Yu, J. L. Huang, and C. M. Lieber, Nature (London) **449**, 885 (2007).
[43]G. Saraf, Y. Lu, and T. Siegrist, Appl. Phys. Lett. **93**, 041903 (2008).
[44]D. Shen, S. Y. Choe, and D. J. Kim, Jpn. J. Appl. Phys., Part 1 **46**, 6755 (2007).